Numerical Solution of a Boundary Value Inverse Problem for the Equation of Unsteady Relaxation Filtration of a Fluid in a Porous Medium

KHOLIYAROV ERKIN, TURAEV DILMUROD, KHAYRULLAYEV ISMATULLA,
KOSIMOV ODILBEK, BURIEV JAVOKHIR
Department of Information Technology and Exact Sciences,
Termez University of Economics and Service,
TERMEZ, 190111,
UZBEKISTAN

Abstract: - In this paper, we solve a boundary value inverse problem for the equation of unsteady relaxation fluid flow in a porous medium under elastic conditions. We applied marching methods, specifically the De Souza and Hensel-Hills methods, to solve the problem. Smoothing splines were used to obtain stable solutions, significantly reducing the error in the numerical solution of the problem. Additional data for the inverse problem are generated based on a quasi-real experiment, ensuring a more reliable reconstruction of the sought-after parameters. We also analyze the influence of smoothing parameters on the accuracy of function reconstruction. Numerical validation of the proposed algorithms using model tests demonstrates their stability in the presence of perturbations in the input data. The obtained results confirm the effectiveness of the developed approach and can be used to solve a wide range of inverse flow problems in heterogeneous porous media.

Key-Words: - boundary value inverse problem, difference scheme, approximation, marching method, solution stability, smoothing splines.

Received: September 11, 2025. Revised: March 14 2026. Accepted: May 16, 2026. Published: July 7, 2026.

1 Introduction

One of the first models of relaxation filtration of a liquid in a porous medium [1] was presented in [2], which takes into account the processes of pressure gradient lag relative to the change in filtration velocity, which allowed for a more accurate description of transient flow regimes. Based on the general assumptions of elastic regime theory, using the continuity equation and Darcy's law, the following equation for piezoconductivity was derived

$$\frac{\partial p}{\partial t} = \varkappa\left(\frac{\partial^2 p}{\partial x^2} + \lambda_p \frac{\partial^3 p}{\partial x^2 \partial t}\right), \varkappa = \frac{k}{\mu(m\beta_f + \beta_c)}, \quad (1)$$

where p - current pressure (MPa); t - time; x - coordinate; λ_p - relaxation time of the pressure gradient; $\varkappa$ - piezoconductivity coefficient; k - permeability coefficient; μ - viscosity coefficient; m - porosity; β_f, β_c - compressibility coefficients of the liquid and the formation, respectively.

In [3], the influence of relaxation phenomena on both the pressure gradient and the filtration velocity is considered. Similar to the approach presented in [2], an equation for non-stationary filtration is obtained, which has the following form:

$$\frac{\partial p}{\partial t} + \lambda_v \frac{\partial^2 p}{\partial t^2} = \varkappa\left(\frac{\partial^2 p}{\partial x^2} + \lambda_p \frac{\partial^3 p}{\partial x^2 \partial t}\right) \quad (2)$$

where λ_v - filtration velocity relaxation time.

Further development of this theory was carried out in works [4], where the filtering models were refined taking into account various relaxation and delay effects. Some integral filtering models, taking into account the memory effects of the medium, were proposed in work, [5]. The fundamental principles of the theory of ill-posed problems are presented in work [6], which serves as a basis for further research in this area. The constructions and theoretical justifications of regularizing gradient algorithms used in iterative regularization methods for solving ill-posed problems are presented in work [7].

In [8], particular attention is paid to boundary value problems, which belong to the class of inverse problems, in which information is redundant on one part of the boundary and insufficient on another. The main approach to solving such problems is based on the quasi-inversion method, which is universal in numerical analysis. The essence of the method lies in the correct modification of the operators included in the problem statement by adding additional differential terms. These terms are typically either sufficiently small (allowing them to tend to zero) or are expressed on the boundary, which eliminates problems with boundary conditions that arise during modification. This adjustment makes it possible to include additional conditions in the statement, in particular those containing unknown parameters. It is noted that operators constructed according to this principle, as a rule, are of higher order.

Anomalous fluids, differing in their rheological characteristics from Newtonian viscous fluids, are widely used in polymer and suspension processing processes and are also found in nature (e.g., some oils, biological fluids, and colloidal solutions), which has led to high applied interest in studying their movement in porous media in the context of problems in the oil, gas, and chemical industries. The work [9] presents a systematic exposition of models, mathematical methods, and the main results of the theory of filtration of homogeneous and heterogeneous anomalous fluids. In addition, it contains a section devoted to the physical properties of the flow of anomalous fluids through porous media, and also discusses the applications of this theory to problems of oil field development.

Recently, increasing attention has been paid to the study of generalizations of models (1), (2) based on the application of fractional differential calculus [10]. In [11], it was shown that fractional differential models of relaxation filtering allow a more complete study of relaxation phenomena compared to models of type (1), (2).

Direct problems for equations (1) and (2) have been studied in considerable detail. However, inverse problems for these models have been insufficiently studied; in particular, a priori estimates of their stability are lacking. Meanwhile, solving inverse problems has important practical significance, as it allows one to reconstruct environmental characteristics and process parameters from limited observations. This necessitates further analysis and the development of methods for solving inverse problems for these models.

In [12], a numerical solution of the boundary inverse problem of fluid filtration for the piezoconductivity equation in porous media under elastic conditions is considered, using marching methods, including the De Souza and Hensel-Hills methods. In [13], a boundary inverse problem associated with the relaxation filtration equation (1) is successfully solved.

This paper considers a boundary value inverse problem for the equation of unsteady relaxation fluid flow in a porous medium, taking into account relaxation phenomena in both the pressure gradient and the filtration velocity. The problem is solved numerically using the De Souza and Hensel-Hills marching methods for various perturbations of the initial data. The stability of the resulting solution is assessed depending on the level of error in these data.

2 Problem Formulation

Now let's consider the formulation of a boundary value inverse problem for the equation of unsteady relaxation fluid flow in a porous medium. The fluid pressure values are specified at points $x = L$ and $x = d$, $x \in (0, L)$. The initial pressure distribution is also known $p(x, 0) = p_0$, $\frac{\partial p}{\partial t}(x, 0) = 0$ where $p_0 = const$. This problem can be applied as a determination of characteristic parameters in an oil producing well (PW) based on the values obtained in an observation well (OW). The problem is reduced to determining the pressure field of region $(0, d)$ and PW $(x = 0)$ based on pressure measurements in OW $(x = d)$. The problem requires finding the liquid pressure in the PW (Figure 1).

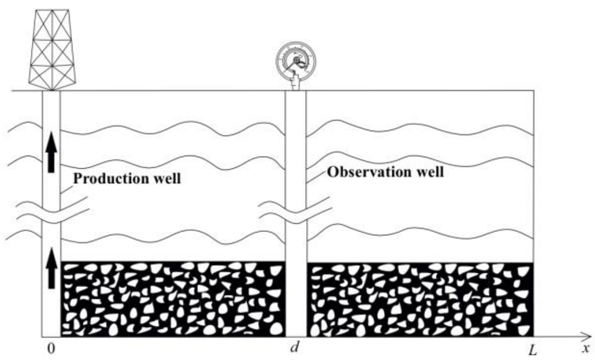

Fig. 1: Schematic representation of a production and observation well (PW, OW)
Source: [13]

Let us formulate the problem in the form of an equation of non-stationary relaxation filtration

$$\frac{\partial p}{\partial t} + \lambda_v \frac{\partial^2 p}{\partial t^2} = \varkappa \left(\frac{\partial^2 p}{\partial x^2} + \lambda_p \frac{\partial^3 p}{\partial x^2 \partial t} \right),$$
$$\varkappa = \frac{k}{\mu(m\beta_f + \beta_c)}, \; t \in (0, t_m], \; 0 < x < L, \tag{3}$$

and additional conditions

$$p(x, 0) = p_0, \; x \in (0, L], \tag{4}$$

$$\frac{\partial p}{\partial t}(x,0) = 0,\ x \in (0, L], \tag{5}$$
$$p(d,t) = z(t),\ t \in (0, t_m], \tag{6}$$
$$p(L,t) = p_0,\ t \in (0, t_m], \tag{7}$$
where t_m is the time during which the process is studied.

To solve the boundary inverse problem, we write out additional data in detail, i.e. $z(t)$ in (6). To do this, we solve the direct problem for equation (3) in the interval $[0, L]$. Therefore, the boundary condition (Darcy's law) is written as follows:
$$v(0,t) = v_0 = -\frac{k}{\mu}\left(\frac{\partial p}{\partial x} + \lambda\frac{\partial^2 p}{\partial x \partial t}\right),\ t \in (0, t_m], \tag{8}$$
where v is the filtration rate;

3 Problem Solution

First, we define the area D, i.e. $D = D_1 \cup D_2 = \begin{Bmatrix} 0 \le x \le d, \\ 0 \le t \le t_m \end{Bmatrix} \cup \begin{Bmatrix} d \le x < \infty, \\ 0 \le t \le t_m \end{Bmatrix}$, then we introduce a grid [14] there
$$\omega_{h\tau} = \left\{ \begin{matrix} (x_i, t_j), x_i = ih, x_n = nh = d, \\ t_j = j\tau, h = \dfrac{L}{N}, \tau = \dfrac{t_m}{M}, \\ i = 0,1,\dots,n,n+1,\dots,N, j = 0,1,\dots,M \end{matrix} \right\}$$
where L is some characteristic length of the formation. First, we approximate problems (3), (4), (5), (7), (8):
$$\frac{p_i^{j+1} - p_i^j}{2\tau} + \lambda_v \frac{p_i^{j+1} - 2p_i^j + p_i^{j-1}}{\tau^2} = \varkappa\left[\frac{p_{i+1}^{j+1} - 2p_i^{j+1} + p_{i-1}^{j+1}}{h^2} + \frac{\lambda_p}{\tau}\left(\frac{p_{i+1}^{j+1} - 2p_i^{j+1} + p_{i-1}^{j+1}}{h^2} - \frac{p_{i+1}^j - 2p_i^j + p_{i-1}^j}{h^2}\right)\right],$$
$$i = 1,2,\dots,N-1,\ j = 0,1,\dots,M-1, \tag{9}$$
$$p_i^0 = p_0,\ i = 0,1,\dots,N, \tag{10}$$
$$\frac{p_i^1 - p_i^0}{\tau} = 0,\ i = 0,1,\dots,N, \tag{11}$$
$$p_N^{j+1} = p_0,\ j = 0,1,\dots,M-1, \tag{12}$$
$$v_0 = -\frac{k}{\mu}\left[\frac{p_0^{j+1} - p_1^{j+1}}{h} + \frac{\lambda}{\tau}\left(\frac{p_0^{j+1} - p_1^{j+1}}{h}\right)\right], \tag{13}$$

Let us write the difference equation (9) as follows:
$$\frac{\varkappa}{h^2}\left(1 + \frac{\lambda_p}{\tau}\right)p_{i-1}^{j+1} - \left[\frac{2\varkappa}{h^2}\left(1 + \frac{\lambda_p}{\tau}\right) + \frac{1}{2\tau} + \frac{\lambda_v}{\tau^2}\right]p_i^{j+1} + \frac{\varkappa}{h^2}\left(1 + \frac{\lambda_p}{\tau}\right)p_{i+1}^{j+1} = \left(\frac{1}{2\tau} - \frac{\lambda_v}{\tau^2}\right)p_i^{j-1} + \left(\frac{2\lambda_v}{\tau^2} + \frac{2\varkappa\lambda_p}{\tau h^2}\right)p_i^j - \frac{\varkappa\lambda_p}{\tau}\left(\frac{p_{i+1}^j + p_{i-1}^j}{h^2}\right),$$

which leads to a system of linear equations
$$A p_{i-1}^{j+1} - C p_i^{j+1} + B p_{i+1}^{j+1} = -F_i^j,$$
$$i = 1,2,\dots,N-1,\ j = 0,1,\dots,M-1 \tag{14}$$

where $A = B = \frac{\varkappa}{h^2}\left(1 + \frac{\lambda_p}{\tau}\right)$,
$$C = \frac{2\varkappa}{h^2}\left(1 + \frac{\lambda_p}{\tau}\right) + \frac{1}{2\tau} + \frac{\lambda_v}{\tau^2},$$
$$F_i^j = \left(\frac{1}{2\tau} - \frac{\lambda_v}{\tau^2}\right)p_i^{j-1} + \left(\frac{2\lambda_v}{\tau^2} + \frac{2\varkappa\lambda_p}{\tau h^2}\right)p_i^j - \frac{\varkappa\lambda_p}{\tau}\left(\frac{p_{i+1}^j + p_{i-1}^j}{h^2}\right).$$

System (14) with (10), (11), (12), (13) is solved by the sweep method.

The difference equation (13) can be written as follows:
$$-\frac{v_0\mu h}{k} = \left(1 + \frac{\lambda_p}{\tau}\right)p_0^{j+1} - \left(1 + \frac{\lambda_p}{\tau}\right)p_1^{j+1} - \frac{\lambda_p}{\tau}\left(p_0^j - p_1^j\right),$$
from here we find
$$p_0^{j+1} = p_1^{j+1} - \frac{v_0\mu h\tau}{k(\tau + \lambda_p)} - \frac{\lambda_p}{\tau + \lambda_p}\left(p_1^j - p_0^j\right).$$

Here we determine the running coefficients, i.e.
$$p_0^{j+1} = \alpha_1 p_1^{j+1} + \beta_1,$$
$$\alpha_1 = 1, \quad \alpha_{i+1} = \frac{B}{C - A\alpha_i}, \tag{15}$$
$$\beta_1 = -\frac{v_0\mu h\tau}{k(\tau + \lambda_p)} - \frac{\lambda_p}{\tau + \lambda_p}\left(p_1^j - p_0^j\right),\ \beta_{i+1} = \frac{A\beta_i + F_i^j}{C - A\alpha_i},$$
$$i = 1,2,\dots,N-1, \quad j = 1,2,\dots,M-1 \tag{16}$$
then we calculate the pressure value
$$p_N^{j+1} = p_0,$$
$$p_i^{j+1} = \alpha_{i+1} p_{i+1}^{j+1} + \beta_{i+1}, \tag{17}$$
$$i = N-1, N-2, \dots, 1, 0,\ j = 1,\dots,M-1.$$

The initial data for the boundary inverse problem are the pressure values at point d, i.e. $z(t_j) = p_n^j$. To evaluate the influence of errors in the initial data on the solution of the boundary inverse problem of the function $z(t)$, we write it as follows
$$z^\delta(t) = z(t) + 2\delta(\sigma(t) - 0.5),$$
where δ - error, $\sigma(t)$ is a uniformly distributed random variable on [0,1]. Figure 2 shows the graphs of the functions $z^\delta(t)$ for different values of d and δ.

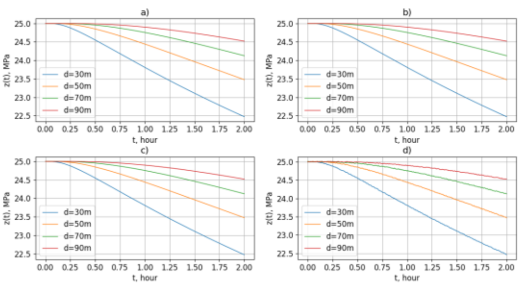

Fig. 2: Graph of the function $z(t)$ at $d = 30\,m, 50\,m, 70\,m, 90\,m$: a) at $\delta = 0$, b) at $\delta = 0.0001$, c) at $\delta = 0.001$, d) at $\delta = 0.01$
Source: created by the authors

To solve the boundary inverse problem we apply the De Souza marching method, [15]. The method uses a purely implicit difference approximation of equation (9). Figure 3 presents the computational stencil of the proposed method, in which, by resolving equation (9) for p_{i-1}^{j+1}, the following expression is obtained.

$$p_{i-1}^{j+1} = \left(2 + \frac{h^2(\tau+2\lambda_v)}{2\varkappa\tau(\tau+\lambda_p)} - 1\right) p_i^{j+1} + \frac{h^2(2\lambda_v-\tau)}{2\varkappa\tau(\tau+\lambda_p)} p_i^{j-1} - \frac{2(h^2\lambda_v+\tau\varkappa\lambda_p)}{\varkappa\tau(\tau+\lambda_p)} p_i^j + \frac{\lambda_p}{\tau+\lambda_p}\left(p_{i+1}^j + p_{i-1}^j\right),\ i = n, n-1, \dots, 1,\ j = 1, \dots, M. \tag{18}$$

From here you can find the value of pressure in the PW.

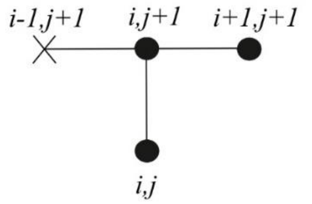

Fig. 3: De Souza's Computational Schematic Template (18)
Source: [13]

The boundary value inverse problem can also be solved using the Hensel-Hills marching method, [15]. We write the approximation of equation (3) as follows:

$$\frac{p_i^{j+1}-p_i^{j-1}}{2\tau} + \lambda_v \frac{p_i^{j+1}-2p_i^j+p_i^{j-1}}{\tau^2} = \varkappa\left[\frac{p_{i+1}^j-2p_i^j+p_{i-1}^j}{h^2} + \frac{\lambda_p}{\tau}\left(\frac{p_{i+1}^j-2p_i^j+p_{i-1}^j}{h^2} - \frac{p_{i+1}^{j-1}-2p_i^{j-1}+p_{i-1}^{j-1}}{h^2}\right)\right], \tag{19}$$

From this we find

$$p_{i-1}^j = \frac{1}{\varkappa\tau(\lambda_p+\tau)}\Big(h^2\lambda_v\left(p_i^{j+1}+p_i^{j-1}-2p_i^j\right) + h^2\frac{\tau}{2}\left(p_i^{j+1}+p_i^{j-1}\right) + \varkappa\lambda_p\tau\left(p_{i-1}^{j-1}-2p_i^{j-1}+p_{i+1}^{j-1}+2p_i^j-p_{i+1}^j\right) + \varkappa\tau^2\left(2p_i^j-p_{i+1}^j\right)\Big), \tag{20}$$
$$i = n, n-1, \dots, 1,\ j = 2, \dots, M-1.$$

From equation (18) we can find the equation where $j = 1$ and $j = M$:

$$p_{i-1}^1 = \frac{Cp_i^1 - Bp_{i+1}^1 - F_i^0}{A}, \tag{21}$$
$$p_{i-1}^M = \frac{Cp_i^M - Bp_{i+1}^M - F_i^{M-1}}{A}, \tag{22}$$
$i = n, n-1, \dots, 1$.

The computational template for equations (20), (21), (22) is shown in Figure 4.

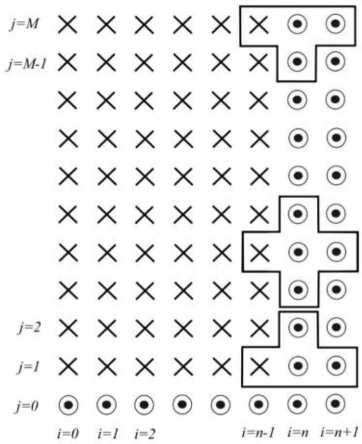

Fig. 4: Computational Scheme Template of the Hensel-Hills Method (20), (21), (22)
Source: [13]

4 Results and Discussion

For the numerical solution of problem (3), (4), (5), (7), (8) the following initial data values were used: $L = 200\,m$, $T = 7200\,s$, $k = 1\cdot10^{-12}\,m^2$, $\varkappa = 3\cdot10^{-1}\,m^2/s$, $p_0 = 25\,MPa$, $\mu = 0.1\cdot10^{-8}\,MPa\cdot s$, $v_0 = 1\cdot10^{-4}\,m/s$, $\lambda_p = 1000\,s$, $\lambda_v = 500\,s$.

In the first stage, numerical results were obtained using the De Souza marching method. Despite the method's sensitivity to input data, with proper parameter settings, it was possible to obtain approximate solutions reflecting the key characteristics of the physical process.

However, with noisy input data, the solution's stability deteriorates, requiring additional regularization. To smooth the solutions and reduce the impact of noise, splines were used, which partially compensated for the method's instability.

Figure 5 and Figure 6 present the results of the numerical and analytical solutions of the function for the parameter value and various values of the distance. As can be seen from Figures 5a), 5b), and 5c), the numerical and analytical solutions almost completely coincide, indicating the high accuracy of the approximate method used. However, Figure 5d) shows a decrease in the stability of the numerical solution, which is associated with an increase in the value of the parameter. To improve the stability of the calculations, the distance was reduced, which made it possible to restore the exact coincidence of the solutions, as shown in Figure 6.

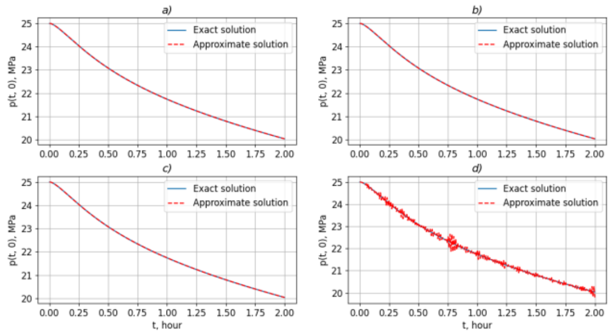

Fig. 5: Results of solving the boundary value inverse problem using the De Souza method for $\delta = 0$: a) at $d = 30\,m$; b) at $d = 50\,m$; c) at $d = 70\,m$; d) at $d = 90\,m$

Source: created by the authors

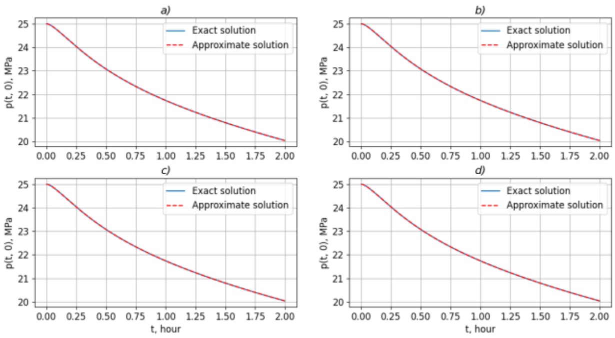

Fig. 6: Results of solving the boundary value inverse problem using the De Souza method for $\delta = 0$: a) at $d = 20\,m$; b) at $d = 25\,m$; c) at $d = 30\,m$; d) at $d = 40\,m$

Source: created by the authors

Figure 7, Figure 8 and Figure 9 show the results of calculations of exact and approximate solutions for different values of δ.

Figure 7 shows the results of calculations of exact and approximate solutions of the function $p(t, 0)$ with $\delta = 0.0001$ for different values of the parameter d. It can be seen from the graphs that with an increase in the value of d, the perturbations in the approximate solution of the boundary inverse problem increase, which indicates a decrease in the stability of the numerical method.

In Figure 7a), for a small value of d, there is almost complete coincidence between the exact and approximate solutions, which indicates the high accuracy and stability of the method.

In Figure 7b), with a moderate increase in d, minor oscillations begin to appear in the approximate solution, but the general behavior of the function is preserved.

In Figure 7c), a further increase in d leads to increased oscillations, which degrades the accuracy of the approximate solution.

In Figure 7d), for large values of d, the approximate solution becomes highly noisy and loses physical interpretability, which indicates a significant loss of stability of the numerical algorithm.

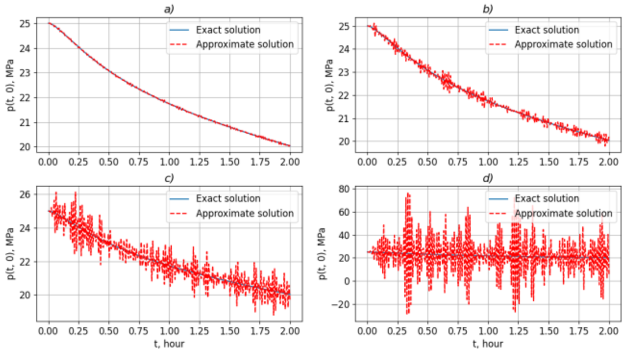

Fig. 7: Results of solving the boundary value inverse problem using the De Souza method for $\delta = 0.0001$: a) at $d = 20\,m$; b) at $d = 25\,m$; c) at $d = 30\,m$; d) at $d = 40\,m$

Source: created by the authors

Figure 8 shows the results of calculating the function $p(t, 0)$ for delta and various values of the parameter d. Compared to the results in Figure 7, the perturbations of the approximate solutions become even more pronounced, indicating an increase in the instability of the inverse problem with increasing δ.

In Figure 8a), for a relatively small value of d, the approximate solution exhibits noticeable fluctuations, but the general shape of the solution is preserved and remains comparable to the exact one.

In Figure 8b), as d increases, the amplitude of oscillations in the approximate solution increases, and deviations from the exact solution become more pronounced.

In Figure 8c), the oscillations become chaotic and the accuracy of the approximate solution is significantly reduced.

In Figure 8d), for large values of d, strong disturbances are observed with sharp jumps reaching hundreds of MPa, which makes the approximate solution unsuitable for practical use due to the loss of stability and physical interpretability.

Figure 9 shows the results of calculating $p(t, 0)$ for $\delta = 0.01$ and various values of the parameter d. Compared to Figure 7 and Figure 8, the approximate solutions exhibit even more pronounced perturbations. This indicates a significant decrease in the stability of the numerical method with increasing δ error, especially for large values of d.

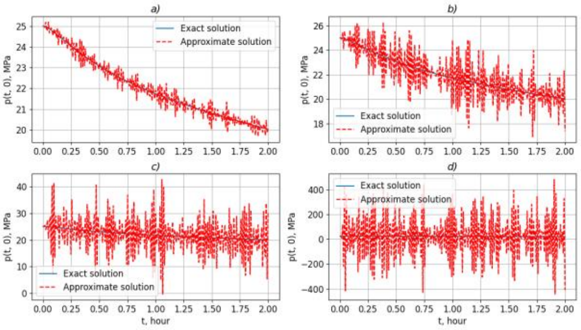

Fig. 8: Results of solving the boundary value inverse problem using the De Souza method for $\delta = 0.001$: a) at $d = 20\,m$; b) at $d = 25\,m$; c) at $d = 30\,m$; d) at $d = 40\,m$

Source: created by the authors

In Figure 9a), even at a relatively small value of d, the approximate solution contains noticeable oscillations, although its amplitude remains within reasonable limits compared to the exact solution.

In Figure 9b) With further increase of d, the oscillations become stronger, the approximate solution deviates from the exact one, and the structure of the graph becomes less predictable.

In Figure 9c) the disturbances become chaotic and resonant in nature, and sudden changes in amplitude are observed that exceed the permissible pressure values.

Figure 9d) For large values of d, the approximate solution completely loses stability: the amplitude of oscillations reaches several thousand MPa, which makes the result physically incorrect and unsuitable for analysis.

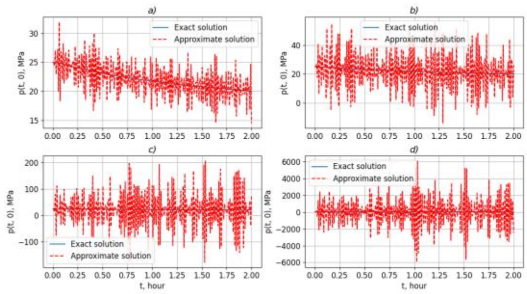

Fig. 9: Results of solving the boundary value inverse problem using the De Souza method for $\delta = 0.01$: a) at $d = 20\,m$; b) at $d = 25\,m$; c) at $d = 30\,m$; d) at $d = 40\,m$

Source: created by the authors

Figure 10, Figure 11 and Figure 12 show the results of calculations of exact and approximate solutions for different values of delta using smoothing splines, [16].

Figure 10 presents the results of calculating the exact and approximate solutions of the function $p(t, 0)$ for a fixed value of the parameter $\delta = 0.0001$ for various values of the parameter d. Approximate solutions of the boundary inverse problem were obtained using smoothing splines, which allows us to evaluate the stability and accuracy of this method.

In Figure 10a), the exact and approximate solutions demonstrate a high degree of agreement. Both $p(t, 0)$ dependencies are characterized by a smooth decrease from 25 MPa to 20 MPa over 2 hours. This indicates that, at this value, smoothing splines provide an accurate reproduction of the solution.

In Figure 10b), the behavior of the solutions is similar to graph a). The differences between the exact and approximate solutions are minimal, which confirms the stability of the smoothing spline method for this value of d.

Figure 10c) shows a slight discrepancy at the initial time $(t = 0)$: the approximate solution exhibits a sharp jump (around 25 MPa), while the exact solution starts with a lower value. However, after this jump, the approximate solution quickly stabilizes and follows the exact solution, decreasing to 20 MPa. This indicates a local instability of the method at the initial time.

In Figure 10d), the approximate solution exhibits significant oscillations. The exact solution remains smooth, highlighting the instability of the approximate solution for a given value of d.

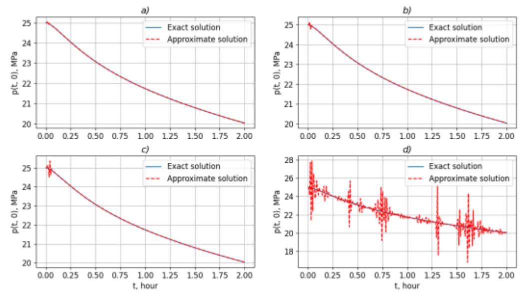

Fig. 10: Results of solving the boundary value inverse problem using the De Souza method with a smoothing spline at $\delta = 0.0001$: a) at $d = 20\,m$, $s = 0.00001$; b) at $d = 25\,m$, $s = 0.00001$; c) at $d = 30\,m$, $s = 0.00001$; d) at $d = 40\,m$, $s = 0.0000005$. Where s is the smoothing parameter

Source: created by the authors

Figure 11 shows the results of pressure calculations $p(t, 0)$ at $\delta = 0.001$ for different values of d. For each graph, both exact solutions and approximate solutions obtained using smoothing splines are shown.

In Figure 11a) it can be seen that for small d the exact solution exhibits an exponential pressure decrease, while the approximate solution obtained using splines shows a more stable behavior.

Figure 11b) confirms similar trends, where increasing d leads to a change in the shape of the curve, but the approximate solution continues to remain stable.

Figure 11c) demonstrates that with further increases in d the exact solution becomes more irregular, while splines successfully smooth out these fluctuations, providing more reliable results.

In Figure 11d) there is a significant discrepancy between the exact and approximate solutions, however, as in the previous cases, smoothing splines can significantly improve the stability of the approximate solution.

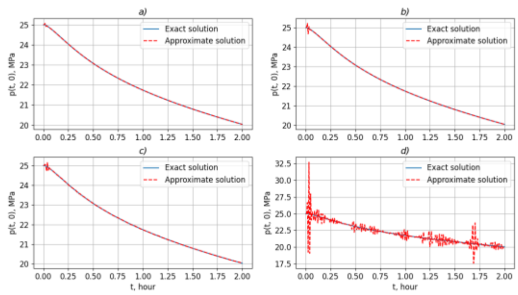

Fig. 11: Results of solving the boundary value inverse problem using the De Souza method with a smoothing spline at $\delta = 0.001$: a) at $d = 20\,m$, $s = 0.0001$; b) at $d = 25\,m$, $s = 0.0001$; c) at $d = 30\,m$, $s = 0.00007$; d) at $d = 40\,m$, $s = 0.00006$
Source: created by the authors

Figure 12 shows the results of pressure calculations $p(t, 0)$ for $\delta = 0.01$ for different values of d. As in previous studies, smoothing splines were used for the analysis, which provide more stable solutions.

In Figure 12a, it is observed that for small values of d, the exact solution exhibits a gradual decrease in pressure. The approximate solution obtained using splines shows a smoother curve, softening the sharp changes.

Figure 12b) confirms the stability of the approximate solution, which retains its shape even with increasing d. This allows us to conclude that smoothing splines are reliable under changing parameters.

Figure 12c) shows that as d increases further, the exact solution begins to oscillate. However, the approximate solution remains stable thanks to the use of splines, demonstrating their effectiveness.

Figure 12d) demonstrates sharp jumps in the exact solution, while the splines continue to provide smoothness and stability. This is especially important for the correct analysis of dynamic processes and the prevention of misinterpretations.

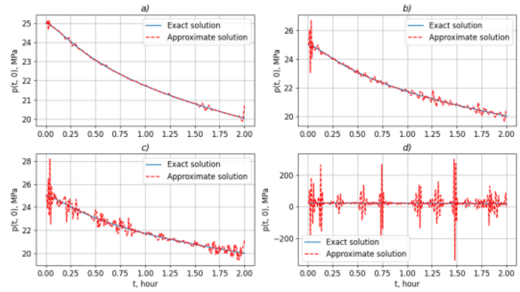

Fig. 12: Results of solving the boundary value inverse problem using the De Souza method with a smoothing spline at $\delta = 0.01$: a) at $d = 20\,m$, $s = 0.006$; b) at $d = 25\,m$, $s = 0.006$; c) at $d = 30\,m$, $s = 0.006$; d) at $d = 40\,m$, $s = 0.005$ *Source: created by the authors*

The next step involved analyzing the numerical solution results obtained using the Hensel-Hills marching method. This method demonstrated high efficiency in solving the boundary value inverse problem, ensuring computational stability and accuracy.

Figure 13 and Figure 14 show the results of calculations of exact and approximate solutions of pressure $p(t, 0)$ at $\delta = 0$ for different values of d.

Figure 13 shows that the exact solutions exhibit a predictable decrease in pressure over time. Approximate solutions also show a similar trend.

In Figure 14, the results are similar, but with different values of d. The exact and approximate solutions remain close to each other, which confirms the reliability of the chosen method.

In both cases, it is observed that at $\delta = 0$, the exact and approximate solutions remain reasonably consistent. This suggests that the approximation methods are effective in the absence of interference.

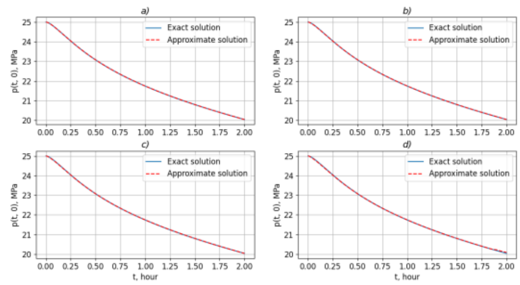

Fig. 13: Results of solving the boundary value inverse problem using the Hensel-Hills method at $\delta = 0$: a) at $d = 30\,m$; b) at $d = 50\,m$; c) at $d = 70\,m$; d) at $d = 90\,m$
Source: created by the authors

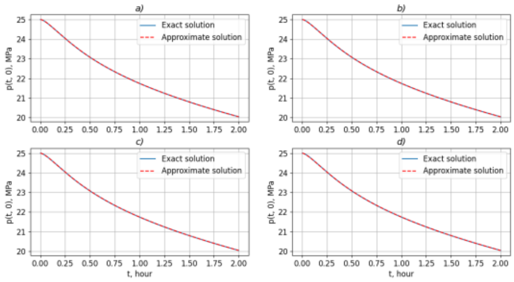

Fig. 14: Results of solving the boundary value inverse problem using the Hensel-Hills method at $\delta = 0$: a) at $d = 20\,m$; b) at $d = 25\,m$; c) at $d = 30\,m$; d) at $d = 40\,m$

Source: created by the authors

Figure 15, Figure 16 and Figure 17 show the results of calculations of exact and approximate solutions for different values of δ.

Figure 15 shows the results of calculations of exact and approximate solutions $p(t,0)$ with $\delta = 0.0001$ for different values of d.

In Figures 15a) – 15c) the exact and approximate solutions are close to each other, which indicates the high accuracy of the method for a small value of d.

Figure 15d) shows pronounced oscillations in the exact solution, while the approximate solution also shows some jumps, highlighting the limitations of the method under conditions where δ is close to zero.

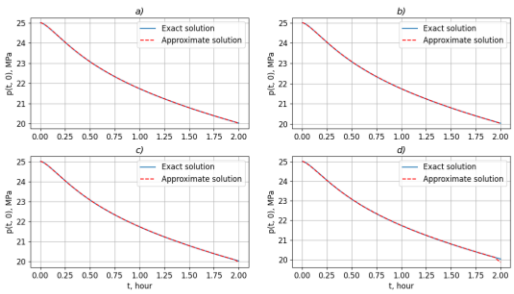

Fig. 15: Results of solving the boundary value inverse problem using the Hensel-Hills method at $\delta = 0.0001$: a) at $d = 20\,m$; b) at $d = 25\,m$; c) at $d = 30\,m$; d) at $d = 40\,m$

Source: created by the authors

Figure 16 shows the results of calculations of exact and approximate solutions $p(t,0)$ for $\delta = 0.001$ for different values of d.

In Figure 16a)-16b) it can be observed that the approximate solution is close to the exact solution.

Figure 16c) demonstrates a further deterioration in the stability of the approximate solution. A significant deviation from the exact solution is observed, especially at later stages. This indicates an increase in error with increasing d.

Figure 16d) shows that the approximate solution has deviated significantly from the exact solution, indicating a critical decrease in stability. This result highlights the importance of analyzing the sensitivity of models to changes in parameters.

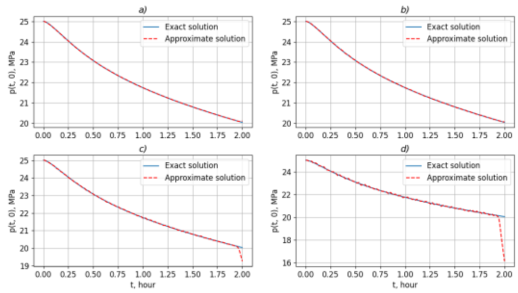

Fig. 16: Results of solving the boundary value inverse problem using the Hensel-Hills method at $\delta = 0.001$: a) at $d = 20\,m$; b) at $d = 25\,m$; c) at $d = 30\,m$; d) at $d = 40\,m$

Source: created by the authors

Figure 17 shows the results of calculations of exact and approximate solutions of $p(t,0)$ for $\delta = 0.01$ for different values of d. As can be seen, the stability of the approximate solution is significantly worse than in Figure 16.

In Figure 17a), it can be noted that the approximate solution exhibits a more pronounced discrepancy with the exact solution compared to the similar subgraph in Figure 16. This indicates a decrease in accuracy with increasing δ value.

In Figure 17b), the discrepancy becomes even more noticeable. The approximate solution begins to deviate from the exact solution more sharply, highlighting the deterioration of the model's stability with increasing δ and d values.

Figure 17c) demonstrates a significant increase in the difference between the approximate and exact solutions. The error in the approximate solution continues to grow, indicating critical sensitivity of the model to parameter changes.

Figure 17d) shows the maximum discrepancy between the approximate and exact solutions. This finally confirms that increasing δ leads to a significant deterioration in the stability of the approximate solution, calling into question its applicability to this problem.

Figure 18, Figure 19 and Figure 20 show the results of calculations of exact and approximate solutions for different values of delta using smoothing splines, [16].

Figure 18 shows the results of calculating the pressure function $p(t,0)$ with the parameter $\delta = 0.0001$ for various values of d. Using smoothing splines, more stable solutions were obtained compared to previous experiments.

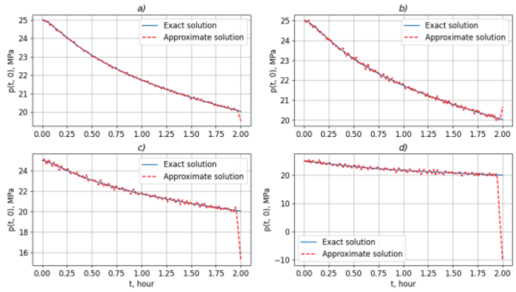

Fig. 17: Results of solving the boundary value inverse problem using the Hensel-Hills method at $\delta = 0.01$: a) at $d = 20\,m$; b) at $d = 25\,m$; c) at $d = 30\,m$; d) at $d = 40\,m$

Source: created by the authors

In Figure 18a)-18c), smoothing splines were not used. Figure 18d) shows that the approximate solution obtained using smoothing splines is virtually identical to the exact solution over the entire time interval. This demonstrates the high stability of the method at small δ values.

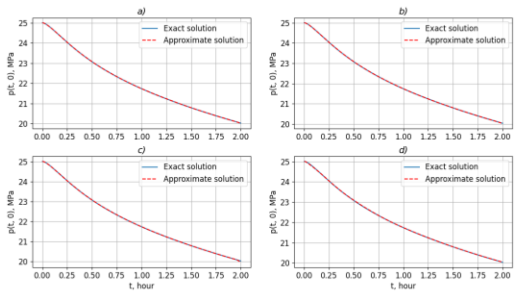

Fig. 18: Results of solving the boundary value inverse problem using the Hensel-Hills method with a smoothing spline at $\delta = 0.0001$: a) at $d = 20\,m$, $s = 0$; b) at $d = 25\,m$, $s = 0$; c) at $d = 30\,m$, $s = 0$; d) at $d = 40\,m$, $s = 0.0001$. Where s is the smoothing parameter

Source: created by the authors

Figure 19 shows the results of calculating the pressure function $p(t, 0)$ with the parameter $\delta = 0.001$ for various values of d. Using smoothing splines, more stable solutions were obtained compared to previous experiments.

In Figures 19a)–19b), smoothing splines were not used. From Figures 19c)–19d), it is evident that the approximate solution obtained using smoothing splines demonstrates good agreement with the exact solution. The stability of the solution has improved significantly compared to similar calculations without splines.

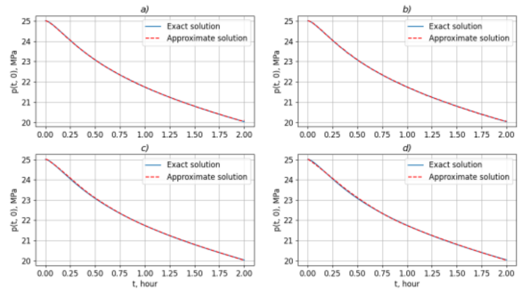

Fig. 19: Results of solving the boundary value inverse problem using the Hensel-Hills method with a smoothing spline at $\delta = 0.001$: a) at $d = 20\,m$, $s = 0$; b) at $d = 25\,m$, $s = 0$; c) at $d = 30\,m$, $s = 0.001$; d) at $d = 40\,m$, $s = 0.001$

Source: created by the authors

Figure 20 shows the results of calculating the pressure function $p(t, 0)$ at $\delta = 0.01$ for various values of d. Using smoothing splines, more stable solutions were obtained compared to previous calculations.

From Figures 20a)-20d) it can be seen that the approximate solution exhibits a high degree of accuracy, which indicates that the use of smoothing splines significantly improves the stability of the calculations as the δ value increases.

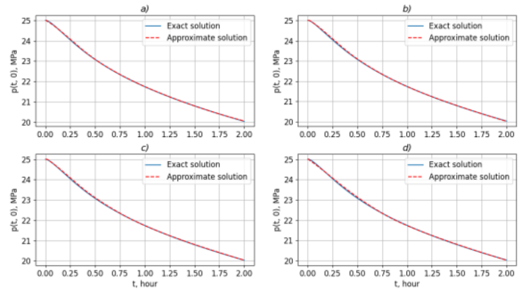

Fig. 20: Results of solving the boundary value inverse problem using the Hensel-Hills method with a smoothing spline at $\delta = 0.01$: a) at $d = 20\,m$, $s = 0.01$; b) at $d = 25\,m$, $s = 0.01$; c) at $d = 30\,m$, $s = 0.01$; d) at $d = 40\,m$, $s = 0.01$.

Source: created by the authors

Table 1 provides a comparative analysis of the RMSE values obtained by the considered marching methods for various values of δ and d.

Table 1. RMSE Comparison of Marching Methods

δ	d	De Souza	De Souza (s)	Hensel–Hills	Hensel–Hills (s)
0	20	1.13e−10	-	1.99e−03	-
0	25	1.72e−10	-	2.16e−03	-
0	30	3.53e−10	-	2.34e−03	-
0	40	7.47e−09	-	2.78e−03	-
1e−4	20	2.79e−02	5.88e−03	3.01e−03	3.01e−03
1e−4	25	1.58e−01	1.56e−02	2.93e−03	2.93e−03
1e−4	30	7.28e−01	4.37e−02	6.56e−03	6.56e−03
1e−4	40	2.00e+01	8.90e−01	1.96e−02	7.36e−03
1e−3	20	3.04e−01	6.27e−03	7.09e−03	7.09e−03
1e−3	25	1.41e+00	2.42e−02	7.59e−03	7.59e−03
1e−3	30	7.33e+00	2.49e−02	7.27e−02	1.54e−02
1e−3	40	1.92e+02	9.17e−01	4.30e−01	1.86e−02
1e−2	20	2.73e+00	6.89e−02	6.11e−02	1.21e−02
1e−2	25	1.43e+01	2.36e−01	8.54e−02	1.93e−02
1e−2	30	7.53e+01	4.46e−01	4.78e−01	1.98e−02
1e−2	40	2.00e+03	6.16e+01	3.25e+00	2.51e−02

Source: created by the authors

5 Conclusion

This paper presents and numerically solves a boundary-value inverse problem for the equation of unsteady relaxation fluid flow in a porous medium. The solution employs marching methods: the De Souza method and the Hensel-Hills method. Although the difference schemes underlying these methods are unstable when solving direct problems, they prove useful when solving inverse problems, where sensitivity to the initial approximation is important. Additional data for the inverse problem are generated based on a quasi-real experiment. The input data contain perturbations simulating random measurement errors. Under such perturbations, the resulting pressure solution is distorted in accordance with the level of the introduced errors. Smoothing splines are used to improve the stability of the numerical solution. With the correct choice of regularization parameters and spline characteristics, the influence of noise can be significantly reduced and a satisfactorily stable solution to the inverse problem can be obtained. A comparative analysis of the results obtained using the two methods shows that the Hensel-Hills method provides more robust and accurate solutions than the De Souza method, especially under noisy input data conditions. The main drawback of the presented methods is the lack of statistical justification. In addition, these methods make it difficult to extend the analysis to two- and three-dimensional problems. At the same time, they allow for the study of a wide range of different problems, whereas marching methods along a spatial coordinate are applicable only in certain cases and are not universally suitable.

References:

[1] Shchelkachev V.N., *Development of oil-bearing formations under elastic conditions*, M.: Gostoptekhizdat, 1959.

[2] Alishaev M.G., On non-stationary filtration with pressure relaxation, *Proceedings of the Moscow Regional Pedagogical Institute named after N.K. Krupskaya, Hydromechanics*, Moscow, 1974, Issue 111.

[3] Alishaev M.G., Mirzadzhanzade A.Kh., On the consideration of delay phenomena in filtration theory, *Publ. of Higher Education Institutions. Oil and Gas*, 1975, No. 6, pp. 71-74, [Online]. https://people.bath.ac.uk/ensdasr/PAPERS/Alishaev-viscoelastic.pdf (Accessed Date: January 20, 2026)..

[4] Molokovich Yu.M., Neprimerov N.N., Pikuza V.I., Shtanin A.V., *Relaxation filtration*, Kazan University Publishing House, 1980. 136 p.

[5] Dinariev, O.Y., Nikolaev, O.V. Relaxation in a low-permeability porous material. Journal of Engineering Physics 58, 65–68 (1990). https://doi.org/10.1007/BF00872700.

[6] Tikhonov A.N., Arsenin V.Ya., *Methods for* solving *ill-posed problems*, M.: Nauka, 1986, 288 p.

[7] Alifanov O.M., Artyukhin E.A., Rumyantsev S.V., *Extreme methods for solving ill-posed problems*, Moscow: Nauka, 1988, 288 p.

[8] Lattès R., Lions J.L., Bellman R., *The method of quasi-reversibility: applications to partial differential equations*, American Elsevier, New York, 1969.

[9] Bernadiner M.G., Entov V.M., *Hydrodynamic Theory of Filtration of Anomalous Liquids*, Nauka, 1975.

[10] Caputo, M. (2000), Models of flux in porous media with memory, Water Resour. Res., 36(3), 693–705, doi: 10.1029/1999WR900299.

[11] B. Khuzhayorov, T.O. Djiyanov, M.S. Zokirov. Generalized relaxation fractional differential model of fluid filtration in a porous medium, *International Journal of Applied Mathematics*, 2024, Volume 37, No. 1, 119–132. http://dx.doi.org/10.12732/ijam.v37i1.10.

[12] Erkin Kholiyarov, Akbar Toyirov, Dilmurod Turaev, Komiljon Gulomkodirov, Solution of boundary inverse problem of fluid filtration in elastic mode, *AIP Conf. Proc.*, 6 May 2024, 3147 (1): 030041. https://doi.org/10.1063/5.0210321.

[13] Kholiyarov E., Turaev D., Buriev J., Numerical solution of boundary inverse problem for fluid relaxation filtration in porous media, *AIP Conference Proceedings, AIP Publishing*, 2024, T. 3244, №. 1. https://doi.org/10.1063/5.0241626.

[14] Samarsky A.A., *Theory of difference schemes*, M.: Nauka, 1989, 616 p.

[15] Beck J.V., Blackwell B., Clair C.R., *Inverse Heat Conduction: Ill-Posed Problems*, Wiley, 1985, 312 p.

[16] Vershinin V.V., Zavyalov Yu.S., Pavlov N.N., *Extremal properties of splines and the smoothing problem*, Novosibirsk: Nauka, 1988.

Contribution of Individual Authors to the Creation of a Scientific Article (Ghostwriting Policy)

The authors equally contributed to the present research, at all stages from the formulation of the problem to the final findings and solution.

Sources of Funding for Research Presented in a Scientific Article or Scientific Article Itself

No funding was received for conducting this study.

Conflict of Interest

The authors have no conflicts of interest to declare that are relevant to the content of this article.